Biochimica et Biophysica Acta 1797 (2010) 865–877

Contents lists available at ScienceDirect

Biochimica et Biophysica Acta

journal homepage: www.elsevier.com/locate/bbabio

Redox-optimized ROS balance: A unifying hypothesis

M.A. Aon [1], S. Cortassa [1], B. O'Rourke *

The Johns Hopkins University, School of Medicine, Institute of Molecular Cardiobiology, Baltimore, MD, USA

ARTICLE INFO

Article history:
Received 25 November 2009
Received in revised form 20 January 2010
Accepted 16 February 2010
Available online 20 February 2010

Keywords:
Mitochondrial membrane potential
Mild uncoupling
Oxidative phosphorylation
Reverse electron transport
Forward electron transport
Redox potential
Hypoxia
Oxidative stress

ABSTRACT

While it is generally accepted that mitochondrial reactive oxygen species (ROS) balance depends on the both rate of single electron reduction of O_2 to superoxide ($O_2^{\cdot-}$) by the electron transport chain and the rate of scavenging by intracellular antioxidant pathways, considerable controversy exists regarding the conditions leading to oxidative stress in intact cells versus isolated mitochondria. Here, we postulate that mitochondria have been evolutionarily optimized to maximize energy output while keeping ROS overflow to a minimum by operating in an intermediate redox state. We show that at the extremes of reduction or oxidation of the redox couples involved in electron transport ($NADH/NAD^+$) or ROS scavenging ($NADPH/NADP^+$, GSH/GSSG), respectively, ROS balance is lost. This results in a net overflow of ROS that increases as one moves farther away from the optimal redox potential. At more reduced mitochondrial redox potentials, ROS production exceeds scavenging, while under more oxidizing conditions (e.g., at higher workloads) antioxidant defenses can be compromised and eventually overwhelmed. Experimental support for this hypothesis is provided in both cardiomyocytes and in isolated mitochondria from guinea pig hearts. The model reconciles, within a single framework, observations that isolated mitochondria tend to display increased oxidative stress at high reduction potentials (and high mitochondrial membrane potential, $\Delta\Psi_m$), whereas intact cardiac cells can display oxidative stress either when mitochondria become more uncoupled (i.e., low $\Delta\Psi_m$) or when mitochondria are maximally reduced (as in ischemia or hypoxia). The continuum described by the model has the potential to account for many disparate experimental observations and also provides a rationale for graded physiological ROS signaling at redox potentials near the minimum.

1. Introduction

Mitochondrial ROS generation has garnered enormous interest and importance in recent years as the scope of mitochondrial function has expanded from the role of powerhouse to the regulation of cell death, physiological signaling, and the ever increasing recognition of the impact of mitochondria on health, disease, aging, and lifespan. A fundamental unanswered question is about the relationship between overall O_2 consumption rate and ROS production [1]. This question lies at the heart of understanding the progression of disease, the free radical theory of aging[2], the "rate living" hypothesis of Pearl [3], and more recently, the regulation of genes governing lifespan [4–6].

Although ROS can be produced in cells by many mechanisms, and in diverse compartments, a large fraction of ROS (up to 90%) can be of mitochondrial origin [7]. Despite the broad significance of mitochondria-derived ROS, there is currently no unifying theory to account for the significant discrepancies existing in results obtained from isolated mitochondria and cells. Consequently, a common tendency is to extrapolate the mechanisms described in the organelle *in vitro* to the intact cell or tissue. The main areas of conflict with respect to the regulation of mitochondrial ROS include: *i*) the relationship between ROS generation, electron transport chain flux and $\Delta\Psi_m$, *ii*) the electron carrier sites from which the ROS arise (e.g. complexes I, II and III), and *iii*) the direction of electron transport during the measurements of ROS production (reverse or forward). An additional important factor is the contribution of the ROS scavenging systems (mitochondrial, cytoplasmic) to the ROS balance, which is frequently overlooked or not investigated in many studies. All of these factors are subject to alterations in the mitochondrial energetic status, and the mechanistic links to ROS balance are incompletely understood.

The importance of the balance between ROS production and scavenging is underscored by observations that oxidative stress can be either protective or damaging in several diseases. For example, during cardiac ischemic preconditioning, in a ROS-dependent mechanism, brief ischemic periods of ischemia can induce protection against cell damage during longer ischemia–reperfusion [8,9]. In contrast, regenerative mitochondrial ROS-induced ROS release [10] can amplify cell injury and also contribute to a state of mitochondrial criticality, defined by the appearance of emergent self-organized behavior in the mitochondrial network [11,12]. The synchronous collapse and/or

* Corresponding author. The Johns Hopkins University, Institute of Molecular Cardiobiology, 720 Rutland Ave., 1060 Ross Bldg., Baltimore, MD 21205-2195, USA. Tel.: +1 410 614 0034; fax: +1 410 502 5055.
E-mail address: bor@jhmi.edu (B. O'Rourke).
[1] These authors contributed equally.

0005-2728/$ – see front matter © 2010 Elsevier B.V. All rights reserved.
doi:10.1016/j.bbabio.2010.02.016

oscillation of $\Delta\Psi_m$ can scale to affect whole cell electrophysiology and contractile function, which may contribute to catastrophic arrhythmias associated with ischemia–reperfusion [13–18].

The concept that mitochondrial ROS generation is maximal when there is little electron flow, high $\Delta\Psi_m$, and a fully reduced NADH pool is pervasive in the literature. Mechanistic support for this idea was obtained in isolated mitochondria under defined conditions, that is, either with mitochondria energized with substrates feeding electrons into complex I in either the forward (glutamate/malate) or reverse (via complex II with succinate) direction. In this state, $\Delta\Psi_m$ and NADH are maximal and the idea that "mild uncoupling" of oxidative phosphorylation could then decrease ROS production was put forward [19,20]. As some have recognized, neither of these conditions are physiological; the mitochondrial NADH pool is never fully reduced in cells [21], except perhaps under hypoxic conditions or with significant damage to complex I, and there are no conditions whereby electron flow could reverse. Notwithstanding, the idea that mild uncoupling can decrease ROS accumulation has become a dogma. In some cases, this might actually be true; however, counterexamples abound. One of them is the fact that oxidative stress typically increases at higher workloads or when intracellular Ca^{2+} rises in most tissues [22–24], two factors that would tend to increase respiration and partially uncouple oxidative phosphorylation. Similarly, cellular pharmacological preconditioning stimuli cause mild uncoupling and an increase in ROS [25], and these effects can be mimicked by low concentrations of the mitochondrial uncoupler, FCCP [26]. In addition, the accumulation of free fatty acids in various pathologies causes mild mitochondrial uncoupling and is associated with increased mitochondrial oxidative stress [27].

Given the potential impact of ROS balance in mitochondria and cells for the design of therapeutic strategies in the context of cardiovascular pathology, neurodegenerative diseases, and cancer, a more coherent and unifying picture is needed. A general model is required to allow more definitive progress in the field and to help reconcile apparently dissenting views. In the present work, we develop a general hypothesis of mitochondrial ROS balance that explains much of the experimental data available from isolated mitochondria and cells based on the idea that ROS overflow can occur at either extreme (i.e. oxidized or reduced) of redox potential. The predictions of the proposed model are validated in isolated mitochondria and cardiomyocytes from the guinea pig heart.

2. Materials and methods

2.1. Mitochondrial isolation from guinea pig hearts

Mitochondria were isolated and handled as described previously [28]. Respiratory Control Ratios (RCR; ratio of state 3 over state 4 respiration with glutamate + malate) of 10 to 20 were obtained using this method.

2.2. Assay of mitochondrial respiration

Mitochondrial respiration was assayed as described previously [28]. Briefly, mitochondrial suspensions (50 to 150 μg of mitochondrial protein) were assayed at 37 °C in a closed chamber of 0.35 ml containing (in mM): 137 KCl, 2 KH_2PO_4, 0.5 EGTA, 2.5 $MgCl_2$, 20 HEPES at pH 7.2 in the presence of complex I (glutamate/malate, G/M, 5 mM each) or complex II (succinate, Succ, 5 mM) substrates. The O_2 concentration in the chamber was monitored by means of a fiber optic O_2 sensor (Ocean Optics, Inc; probe tip diameter = 1 mm) in which the fluorescence emission at 600 nm of a ruthenium compound is quenched by O_2. Calibration of the fiber optic O_2 sensor is described in [28]. Mitochondrial protein was determined using the Bicinchoninic acid method, BCA™ protein assay kit (Pierce, IL).

2.3. Other bioenergetic variables

Independently of respiration measurements, several other variables indicating the mitochondrial physiological status were monitored simultaneously with a spectrofluorometer (Photon Technology, Inc.) utilizing the same medium above for measuring respiration, and a multidye program for simultaneous online monitoring of different fluorescent probes. NAD(P)H, $\Delta\Psi_m$, and mitochondrial swelling were determined as described in [28]. Briefly, NAD(P)H was monitored by exciting mitochondrial suspensions at 340 nm and collecting the emission at 450 nm whereas mitochondrial volume was assessed by light scattering (90° side scatter; excitation wavelength, $\lambda_{exc} = 520$ nm, emission wavelength, $\lambda_{em} = 585$ nm). Mitochondrial $\Delta\Psi_m$ was recorded using tetramethylrhodamine methyl ester (TMRM; 100 nM) and applying the ratiometric method described in [29] that utilizes two λ_{exc} at 546 nm and 573 nm while recording the λ_{em} at 590 nm.

2.4. Redox status and ROS detection

In addition to NAD(P)H as an indicator of the redox status of the mitochondrial matrix, we also monitored reduced glutathione (GSH). The latter was detected as glutathione S-bimane, GSB (the fluorescent adduct obtained after the reversibly glutathione S-transferase catalyzed reaction between monochlorobimane, MCB + GSH ⇔ GSB) [30,31]. The validation of the production and detection of GSB ($\lambda_{em} = 390$ nm; $\lambda_{exc} = 480$ nm) was performed with purified glutathione S-transferase (GST, from rabbit liver, Sigma) to catalyze the *in vitro* reaction of GSH and MCB at 37 °C. Mitochondria (3–4 mg of mitochondrial protein) were loaded with 20 μM MCB in the suspension solution containing 75 mM sucrose and 225 mM mannitol for at least 20 min at room temperature (protected from light, with occasional shaking). After loading, the excess dye was washed out by centrifugation (twice, 6,500 rpm for 1.5 min) in an Eppendorf centrifuge (Eppendorf AG, Hamburg, Germany).

The two different ROS species superoxide, $O_2^{\bullet -}$, and hydrogen peroxide, H_2O_2, were detected utilizing MitoSOX™ (Invitrogen) and the Amplex Red (ARed) kit, respectively, from Invitrogen (Carlsbad, CA). Resorufin, the fluorescent product obtained in the ARed assay after oxidation by H_2O_2 was monitored at $\lambda_{exc} = 530$ nm and $\lambda_{em} = 590$ nm, and MitoSOX at $\lambda_{exc} = 396$ nm and $\lambda_{em} = 580$ nm. Mitochondria (3–4 mg of mitochondrial protein) were loaded with 4 μM MitoSOX in the suspension solution containing 75 mM sucrose and 225 mM mannitol for at least 20 min at room temperature (protected from light, with occasional shaking). After loading, the excess dye was washed out by centrifugation (twice, 6,500 rpm for 1.5 min) in an Eppendorf centrifuge (Eppendorf AG, Hamburg, Germany).

Mitochondria loaded with the different fluorescent probes were preserved on ice all throughout the experiment.

Considering that O_2 can be converted into H_2O_2 or H_2O with a different number of electrons involved, as follows:

$$O_2 + 2H^+ + 2e^- \rightarrow H_2O_2$$

$$O_2 + 4H^+ + 4e^- \rightarrow 2H_2O$$

we calculated the percentage of O_2 consumed diverted to H_2O_2 production as:

$$H_2O_2(\%\, of\, O_2\, consumed) = (H_2O_2(\text{pmol/min})) \div (O_2(\text{nmol/min})*1000(\text{pmol/nmol}))*100.$$

2.5. Cardiomyocyte isolation and fluorescent probes

Myocytes (which were stored in DMEM for at least 2 h) were handled as described in Aon et al. [30]. Briefly, the cells were loaded

with the fluorescent probes 5-(-6)-chloromethyl-2′,7′-dichlorohydrofluorescein diacetate (CM-H_2DCFDA, 2 μM) and 2 μM MitoSOX (Invitrogen-Molecular Probes, Eugene, OR) on the stage of the microscope for at least 20 min at 37 °C to monitor simultaneously H_2O_2 and $O_2^{\bullet-}$ respectively. Fluorescent compounds that are membrane impermeable (e.g. CM-H_2DCFDA) are loaded in their respective acetoxymethyl ester forms, which are cleaved in intracellular compartments by native esterases. We have optimized several parameters that facilitate the accurate detection of MitoSOX by two-photon microscopy, including the specific excitation wavelength used and the dye concentration, in order to avoid non-specific staining of nucleic acids. The possibility of an effect of DTT on ROS detection by the CM-H_2DCFDA and/or MitoSOX probes was ruled out by control experiments. Each one of the probes was incubated in the absence or presence of 100 μM DTT in a cuvette, and the spectrum and maximal oxidized fluorescence was monitored after addition of 10 μM H_2O_2 or 10 μM KO_2, a superoxide donor (see Fig. S5 and S6 in Supplementary material). The properties and responses of the probes were not altered by DTT.

2.6. Kinetic experiments with intact cardiomyocytes

Kinetic experiments with intact cardiomyocytes were carried out at 37 °C in a thermostatically controlled flow chamber mounted on the stage of the upright microscope (Nikon E600FN) attached to the multiphoton laser scanning system. A constant flow was controlled with a peristaltic pump. CM-H_2DCFDA- and MitoSOX-loaded living cardiomyocytes were perfused with normal modified Tyrode's solution containing 1 mM Ca^{2+} and 10 mM glucose in the absence or presence of nanomolar concentrations of FCCP as indicated.

3. Results

In the first part of the study, ROS balance is characterized in isolated mitochondria in both forward electron transport mode (FET) and in reverse mode (RET), and in different energetic states, i.e. state 4 and state 3 respiration (as defined in [32]). We then test the central hypothesis (see below) by varying the redox status in isolated mitochondria or intact cardiomyocytes. The redox environment of the pyridine nucleotide pool is altered by applying low concentrations of the mitochondrial uncoupler FCCP and the thiol redox potential is varied by adjustment of the GSH/GSSG ratio.

3.1. Hypothesis: redox-optimized ROS balance

The main hypothesis is that the extent of ROS imbalance is defined by the overall intracellular redox environment, which includes the redox couples involved in electron transport (NADH/NAD^+, QH_2/QH) and those involved in antioxidant pathways (NADPH/$NADP^+$, GSH/GSSG), and that oxidative stress can occur at either extreme of redox potential, that is, when the intracellular environment is either highly reduced or highly oxidized, as illustrated in Fig. 1. Physiological ROS signaling occurs within a range close to the minimum of the curve.

As one deviates from the minimum, the extent of ROS overflow in the system (reflected as an increased level of detectable free radicals) is governed by completely different mechanisms at the two redox extremes. As the redox environment becomes more reduced (towards the right hand side of the plot), ROS overflow increases because ROS ($O_2^{\bullet-}$, H_2O_2) production (blue line) will be favored and will exceed the scavenger capacity, even though the latter is at its maximum level (green line), whereas at oxidized redox potentials (left hand side), ROS overflow occurs as a consequence of depletion of the ROS scavenger pool.

The redox environment – defined by the set of linked redox couples found in a biological fluid, organelle, cell, or tissue – can be determined from the summation of the products of the reduction potential and reducing capacity of the linked redox couples present ([33]; see also below):

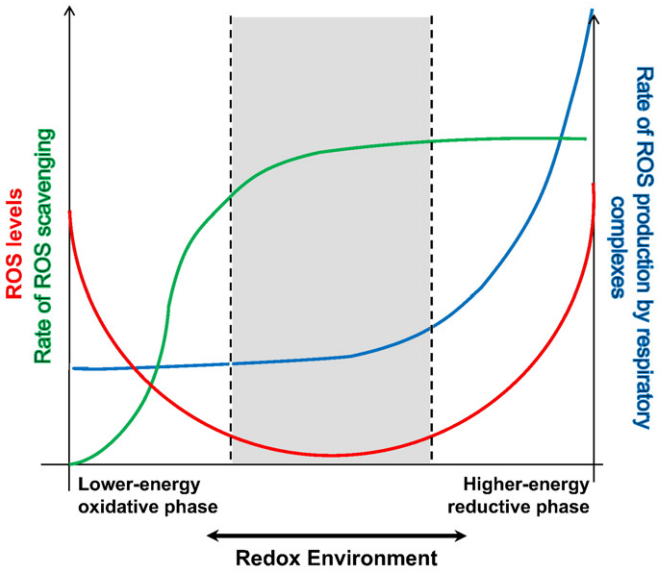

Fig. 1. The redox-optimized ROS balance hypothesis. The plot illustrates that the extent of ROS imbalance is defined by the overall intracellular and intramitochondrial redox environments (see text and Fig. 2). Physiological ROS signaling (denoted between dashed lines) occurs within a range close to the minimum of the overall (red) curve that corresponds to intermediate values of the redox environment. Oxidative stress can happen at either extreme of redox potential, that is, when the intracellular and/or intramitochondrial environments are either highly reduced or highly oxidized. Away from the minimum, the extent of ROS overflow in the system is governed by completely different mechanisms at the two redox extremes. Under a more reduced redox environment (towards the right hand side of the plot), ROS overflow increases because ROS ($O_2^{\bullet-}$, H_2O_2) production (blue line) will be favored, exceeding the scavenger capacity, even though the latter is at its maximum level (green line). At more oxidized redox potentials (left hand side), ROS overflow occurs as a consequence of depletion of the ROS scavengers pool. See text for further details.

$$Redox\,environment = \sum_{i=1}^{n(couple)} E_i \times [reduced\,species]_i \quad (1)$$

where E_i is the half-cell reduction potential (Nernst potential) for a given redox pair and $(\text{reduced species})_i$ is the concentration of the reduced species in that redox pair.

The central tenet of the hypothesis is that the control of ROS levels will shift, in isolated mitochondria or cells, depending on both the specific redox environment and the physiological situation, in particular, the energetic status. A corollary of the hypothesis is that different cell types and tissues will display different minima of ROS levels, shifted towards the left or the right according to the redox scavenging capacity, respiratory, and ROS production fluxes able to be sustained.

3.2. Redox potential

NADH/NAD^+, NADPH/$NADP^+$, GSH/GSSG, thioredoxin (Trx$(SH)_2$/TrxSS), and glutaredoxin (Grx$(SH)_2$/GrxSS) are the principal redox couples involved in intracellular ROS balance, and separate, but interacting, pools are present in the cytoplasm, mitochondrial intramembrane space, and mitochondrial matrix (Fig. 2). They fulfill different specific functions in cellular metabolism. For example, NADPH is the main electron donor for biosynthetic reactions and thiol pool reduction, NAD^+ is the main electron acceptor in catabolic pathways, and NADH is the key electron donor for oxidative

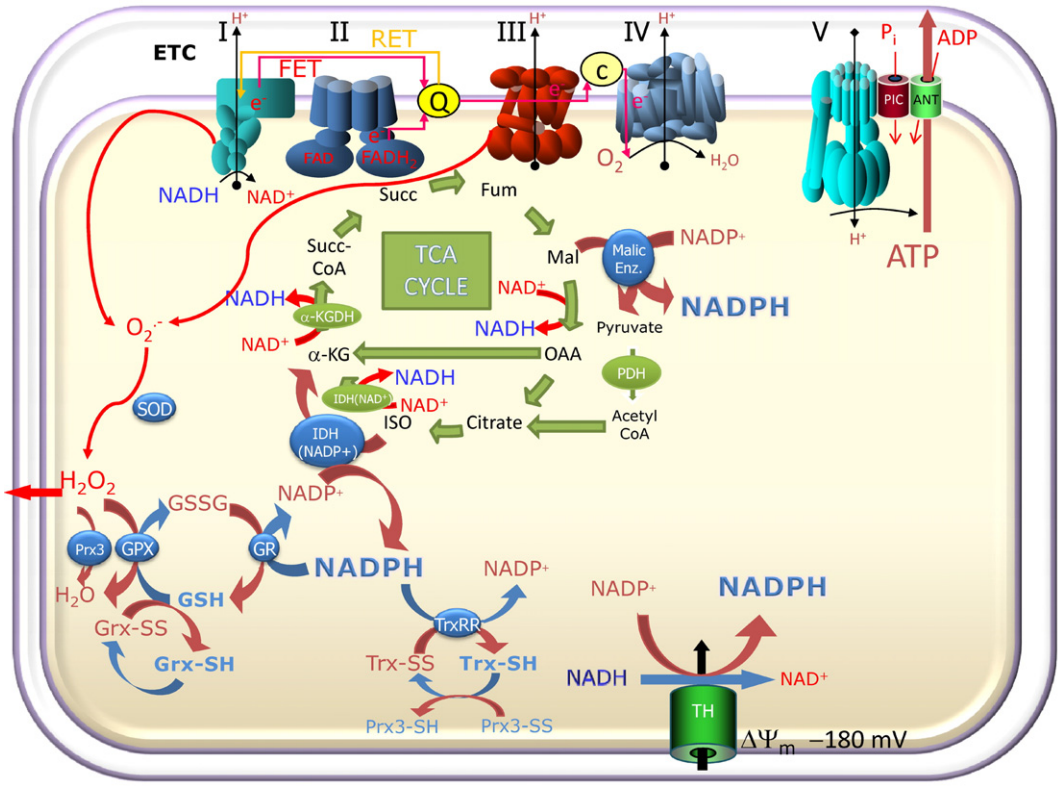

Fig. 2. Moiety-conserved redox cycles linking metabolic and antioxidant pathways in mitochondria. $O_2^{\bullet-}$ produced by the mitochondrial electron transport chain through reverse- or forward-electron transport (RET or FET) is dismutated to H_2O_2 by superoxide dismutase (SOD). The reduced redox environment is controlled by several systems, including the large capacity glutathione system (GSH, GSSG), the glutaredoxin (Grx) system, and the thioredoxin (Trx) system, responsible for the reduction of selected protein targets such as peroxiredoxin (Prx) and ribonucleotide reductase. GSH and Trx are both essential for the detoxification of H_2O_2 via glutathione peroxidase (GPX) and Prx enzymes, respectively. Mitochondrial catalase may also contribute to H_2O_2 scavenging (not shown). Different isoforms of these enzymes are present in the cytosol and in the mitochondrial matrix; however, in both compartments, their redox state depends on maintaining the negative reduction potential of NADPH (>−350 mV). The NADPH/$NADP^+$ redox couple is, in turn, kept in the reduced state through the metabolic pathways of the cell through a close relationship between oxidative metabolism, electron transport, and antioxidants. In the matrix, three major enzymes involved in NADPH regeneration are the NAD(P) transhydrogenase (TH; which catalyzes the transfer of electrons between NADH and $NADP^+$ at the expense of the protonmotive force), the $NADP^+$-dependent isocitrate dehydrogenase (IDH-$NADP^+$) and Malic enzyme; the latter two are dependent on TCA cycle intermediates. Hence, any change in oxidative phosphorylation could also affect the antioxidant pathways.

phosphorylation. A convenient way to quantify the redox potential of a redox couple is through the Nernst potential, as follows:

$$E = E' - \frac{RT}{nF}\log\left(\frac{[Reduced\,form]}{[Oxidized\,form]}\right) \quad (2)$$

where E stands for the electrochemical potential of the hemi-redox reaction of the couple; E' is the redox potential under standard conditions (25 °C, pH 7.0, 1 bar, expressed below in mV units); R, the universal gas constant; T, temperature in Kelvin degrees; n, the number of electrons required to reduce the oxidized form of the couple; and F, the Faraday constant that stands for the charge of a mole of electrons. For example, in the case of the couple NADH/NAD^+, for the half-cell reaction $NAD^+ + H^+ + 2e^- \rightarrow$ NADH, the redox potential is described by:

$$E = -320 - \frac{59.2}{2}\log\left(\frac{[NADH]}{[NAD^+]}\right) \quad (3)$$

Thus, when (NADH:NAD^+) is 5, the redox potential will be −341 mV.

3.3. ROS balance in heart mitochondria under RET or FET conditions

ROS production is profoundly affected by the substrates utilized to energize the mitochondria and the rate and direction of electron transport in the respiratory chain. When electron transport is driven in the physiological forward mode (FET) in the presence of the NAD^+-linked substrates glutamate/malate (G/M), mitochondrial ROS overflow is negligible (that is, any ROS produced are quickly scavenged and cannot be detected by our reporters). In contrast, succinate-supported reverse electron flow (RET) triggers a robust increase in the release of mitochondrial ROS. We first investigated the role of the energy state on ROS release. $\Delta\Psi_m$, NADH, swelling (90° light scattering), and H_2O_2 production (ARed) were simultaneously monitored in freshly isolated mitochondria from guinea pig heart in an isotonic KCl-based assay medium. When energized with either 5 mM each of G/M, or 5 mM succinate (Succ), under state 4 conditions, an immediate increase in $\Delta\Psi_m$ by ~30–50 mV, paralleled by reduction of the NADH pool (Fig. 3A) and low-amplitude swelling (Fig. 3B and C) was observed.

H_2O_2 release to the medium during state 4 respiration was six-fold higher for Succ than for G/M (Fig. 4A). Upon ADP (1 mM) addition to energized mitochondria, the state 4→state 3 transition was associated with partial depolarization of $\Delta\Psi_m$ (~30 mV), NADH oxidation (Fig. 3A), and contraction (Fig. 3B and C). ROS release to the medium was drastically decreased, both under RET (~12-fold) and FET (~2-fold) (Figs. 3A, D, E and 4A).

Mitochondrial respiration, measured in parallel experiments following an identical protocol (Fig. 3), increased substantially after ADP addition, with state 3:state 4 respiratory control ratios (RCR ± SEM) of 30.7 ± 5.4 and 9.1 ± 2.2 ($n = 6$; $p < 0.01$) for G/M and Succ (Fig. 4B),

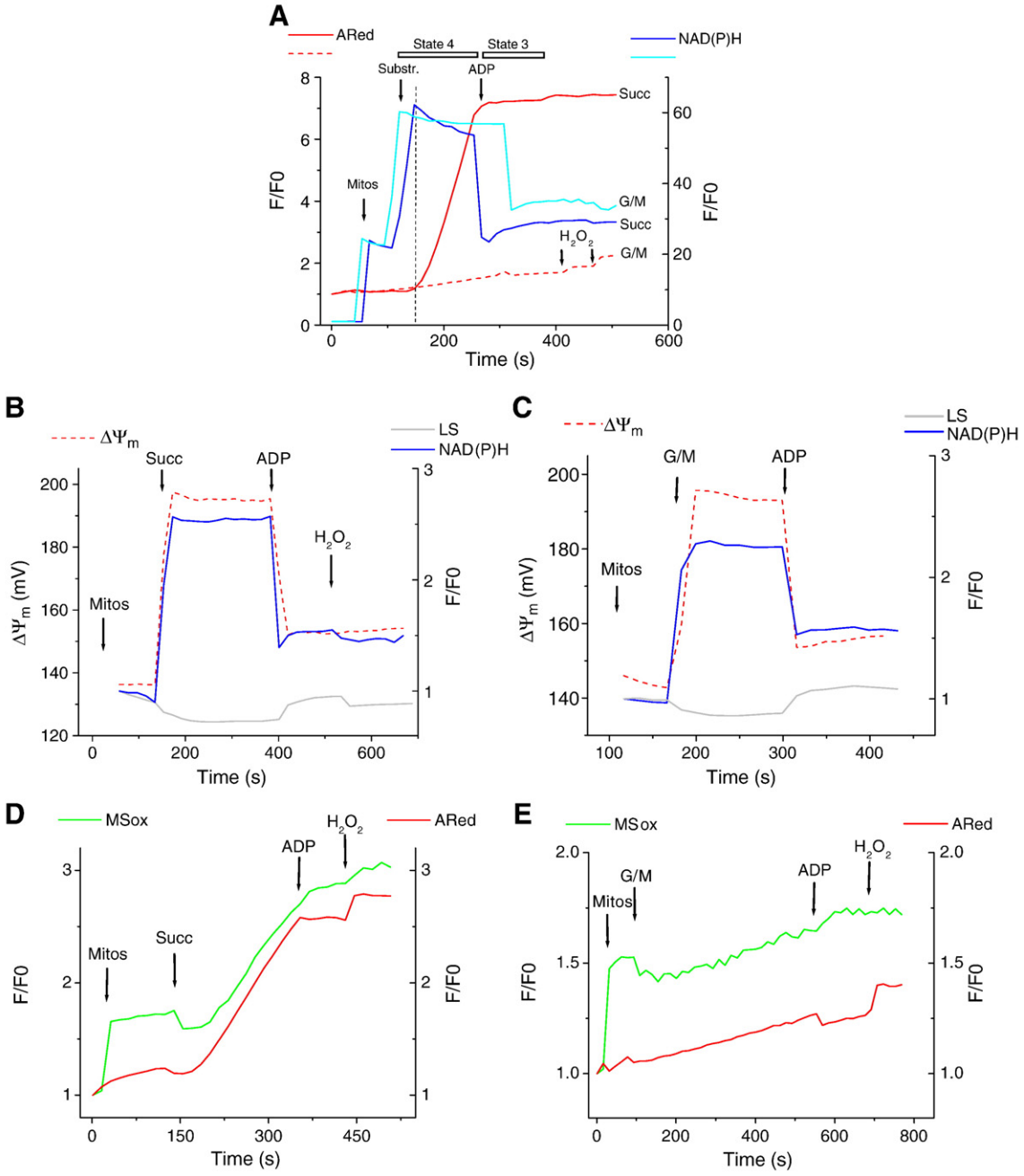

Fig. 3. ROS balance under FET and RET. Simultaneous monitoring of mitochondrial ROS (H_2O_2 with ARed, and $O_2^{\bullet-}$ with MitoSOX; MSox), $\Delta\Psi_m$, and NAD(P)H, during state 4 and the state 4→ state 3 transition in freshly isolated guinea pig heart mitochondria. The forward mode (FET) of electron transport occurs in the presence of the NAD^+-linked substrates glutamate/malate (G/M, continuous lines) whereas reverse electron flow (RET) happens with succinate (Succ, dashed lines)-supported respiration (see text and Materials and methods for further details). A) Isolated mitochondria were resuspended (100–200 μg mitochondrial protein) in the cuvette of a spectrofluorometer containing 2 ml isosmotic 137 mM KCl-based assay medium in the presence of ARed with constant stirring at 37 °C (see Materials and methods). At the indicated times, 5 mM glutamate-K^+/malate-Na^+ or 5 mM Succ (first arrow), or 1 mM ADP (second arrow), were added. NAD(P)H and ROS recordings are shown. Mitochondrial ROS overflow is negligible with G/M (dashed line) but Succ (continuous line) triggers a robust increase in measured H_2O_2 by ARed. Notice the similar degree of NAD(P)H reduction both under FET and RET, and that H_2O_2 starts to increase after the maximal degree of NAD(P)H reduction is attained (vertical dashed line). At the end of the experiment 50 nM H_2O_2 is always added for calibration purposes as well as determining that the ARed system is active under the specified conditions. B, C) Represented are $\Delta\Psi_m$, NAD(P)H, and 90° light scattering, with mitochondria analyzed under similar conditions as in panel A. Notice that on substrate addition, mitochondria respond with low-amplitude swelling (grey trace), $\Delta\Psi_m$ polarization by ~40 mV (dashed red trace) and a 2–2.5-fold NAD(P)H pool reduction (blue trace) whereas ADP addition has the opposite effect, i.e., a volume decrease, $\Delta\Psi_m$ depolarization, and NAD(P)H oxidation (see text for further details). D, E) MitoSOX-loaded mitochondria (see Materials and methods) were analyzed with the same protocol described in panel A in the presence of ARed under RET (D) or FET (E). Notice the parallel increase of $O_2^{\bullet-}$ (MSox) in the matrix, and extra-mitochondrial H_2O_2 (ARed). Key to abbreviations: MSox, MitoSOX; ARed, Amplex Red; G/M, glutamate/malate; Succ, succinate; Mitos, mitochondria.

respectively. The lower RCR registered in the presence of Succ is due to a higher state 4 respiration. In state 4, the H_2O_2 flux represents 1.4% or 0.6% of the O_2 consumption using 5 mM Succ or G/M, respectively, as substrate (Fig. 4A and B). In state 3, the H_2O_2 production represents only a very small fraction 0.016% of the O_2 consumed in the presence of either substrate (Fig. 4A).

Mitochondria loaded with MitoSOX were employed to detect, simultaneously, $O_2^{\bullet-}$ production in the matrix and H_2O_2 (with ARed) in the incubation medium. Mitochondria exhibited a parallel increase in both ROS, suggesting a precursor–product relationship, and also indicating that H_2O_2 release was not diffusion limited (Fig. 3D and E). Strikingly, the production of both matrix generated $O_2^{\bullet-}$ and released

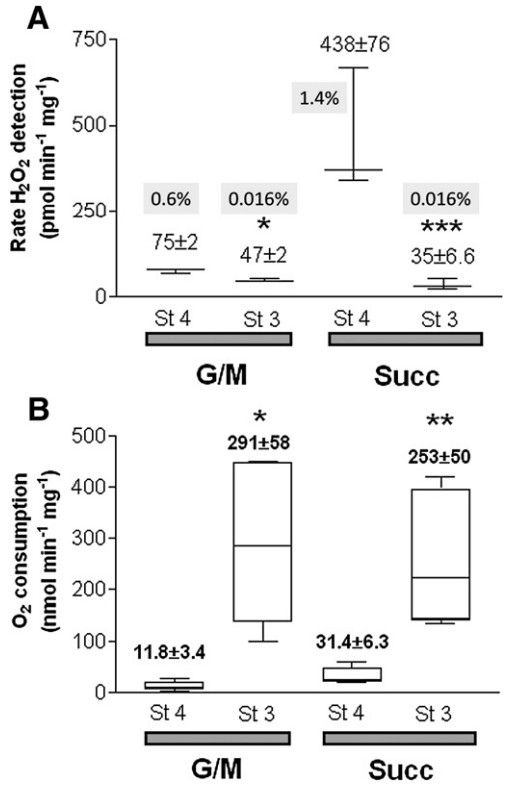

Fig. 4. Rates of ROS production and O_2 consumption under FET and RET. Freshly isolated mitochondria from guinea pig heart were resuspended and analyzed as described in Materials and methods and the legend of Fig. 3. A) Under FET (G/M) and RET (Succ), H_2O_2 and several other bioenergetic variables (e.g. $\Delta\Psi_m$, NAD(P)H) were monitored simultaneously with a spectrofluorometer (see legend Fig. 3 and Materials and methods). B) In parallel, and under similar conditions, O_2 measurements were performed. Mitochondrial respiration was measured in state 3 (St3) and state 4 (St4). Shown are the results obtained with H_2O_2 (A) and O_2 (B) specific fluxes. The numbers in grey represent the H_2O_2 detected as a percentage of the O_2 consumed (see Materials and methods). The number of samples, n, analyzed was $n=4$ (2 experiments) and $n=6$ (2 experiments) for panels A and B, respectively. $^{*}p<0.05$; $^{**}p<0.01$; $^{***}p<0.001$.

H_2O_2 under RET or FET was halted upon ADP addition and the transition to state 3 (Figs. 3–6). These results are consistent with previous reports indicating that mitochondria with high $\Delta\Psi_m$ and a highly reduced NADH/NAD$^+$ ratio can release significant amounts of ROS, but under a load, that is, when ADP is present (the normal physiological state), very little ROS is released.

3.4. Influence of the thiol redox scavengers on mitochondrial ROS overflow

In permeabilized cardiomyocytes, we have previously shown that the interplay between the extra-mitochondrial GSH:GSSG ratio and GSH regeneration in the mitochondrial matrix determines the rate of ROS accumulation [30]. Therefore, we investigated the role of the GSH:GSSG ratio on the mitochondrial ROS balance in isolated cardiac mitochondria.

As depicted in Fig. 5A and C, a high GSH:GSSG ratio of 300:1, which, when present in permeabilized cardiomyocytes, almost eliminates mitochondrial ROS accumulation [30], decreased mitochondrial H_2O_2 release by ~40% under conditions of either RET or FET, assessed in the presence of the complex III inhibitor, antimycin A (5 μM AA). In the case of RET, the state 4→3 transition elicited by ADP still drastically decreased the rate of ROS accumulation, as did rotenone treatment (Fig. 5A). A similar decrease in H_2O_2 release with ADP was observed at the relatively more oxidized GSH:GSSG ratio of 150:1 (Fig. 5A). Under RET, at 150 or 300 GSH:GSSG, there was

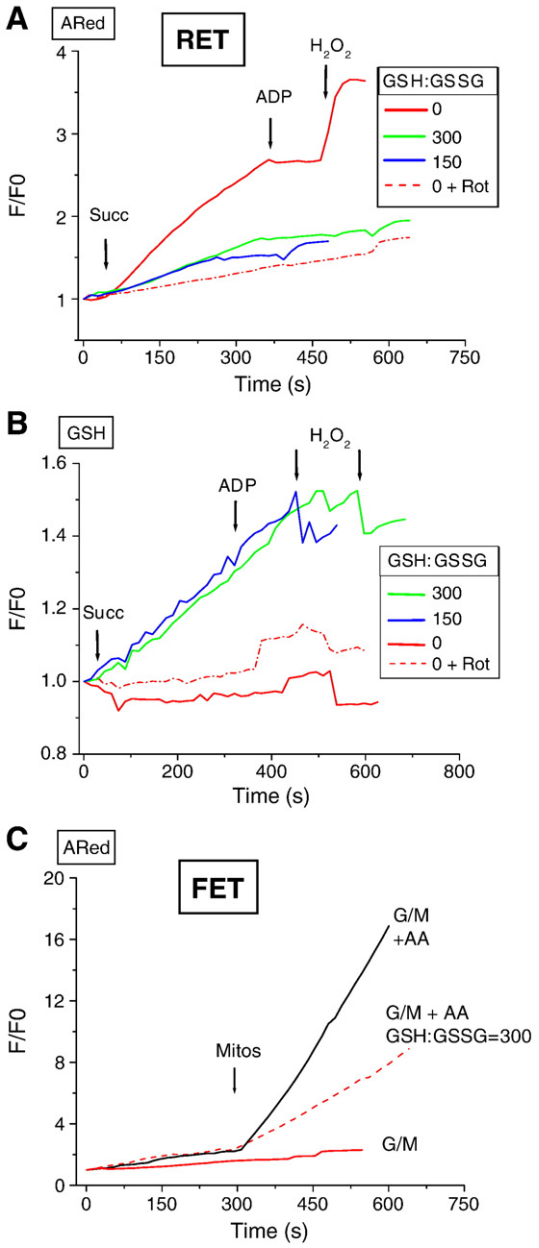

Fig. 5. Effect of the exogenous GSH:GSSG ratio on the mitochondrial ROS balance under FET and RET. Freshly isolated mitochondria from guinea pig heart were loaded with the GSH fluorescent reporter MCB, and preincubated at a fixed GSH:GSSG ratio of 300 or 150 in the extra-mitochondrial space. The GSH:GSSG ratio was varied by changing the GSSG concentration while keeping GSH constant at 3 mM. Mitochondria were analyzed as described in the legend of Fig. 3 under RET (A, B) and FET (C). The complex I origin of ROS under RET was ascertained by preincubating mitochondria with 1 μM rotenone. Under FET, mitochondrial ROS production was analyzed in the presence of 5 μM antimycin A. Shown are the results obtained in a representative experiment. A, C) Notice the decrease in ROS levels detected in the presence of GSH:GSSG either under RET or FET (in pmol H_2O_2 min^{-1} mg^{-1} protein (±SEM, $n=3$, 2 experiments): Succ: control = 666 ± 62, GSH:GSSG(300:1) = 420 ± 31; G/M: control = 104 ± 9, AA = 687 ± 53, GSH:GSSG(300:1) + AA = 414 ± 22), and (B) the increase in intramitochondrial GSH. Key to symbols: AA, antimycin A; Rot, rotenone.

a similar increase in the concentration of the reduced glutathione reporter, glutathione S-bimane (GSB; formed from the reaction of GSH with monochlorobimane) in the matrix. The GSB increase was unaffected by ADP addition (Fig. 5B). This data supports the idea that, even in isolated mitochondria, ROS balance depends on both the rate of production and the antioxidant capacity [34]. Interestingly, the decrease in the ROS release in these experiments was associated with

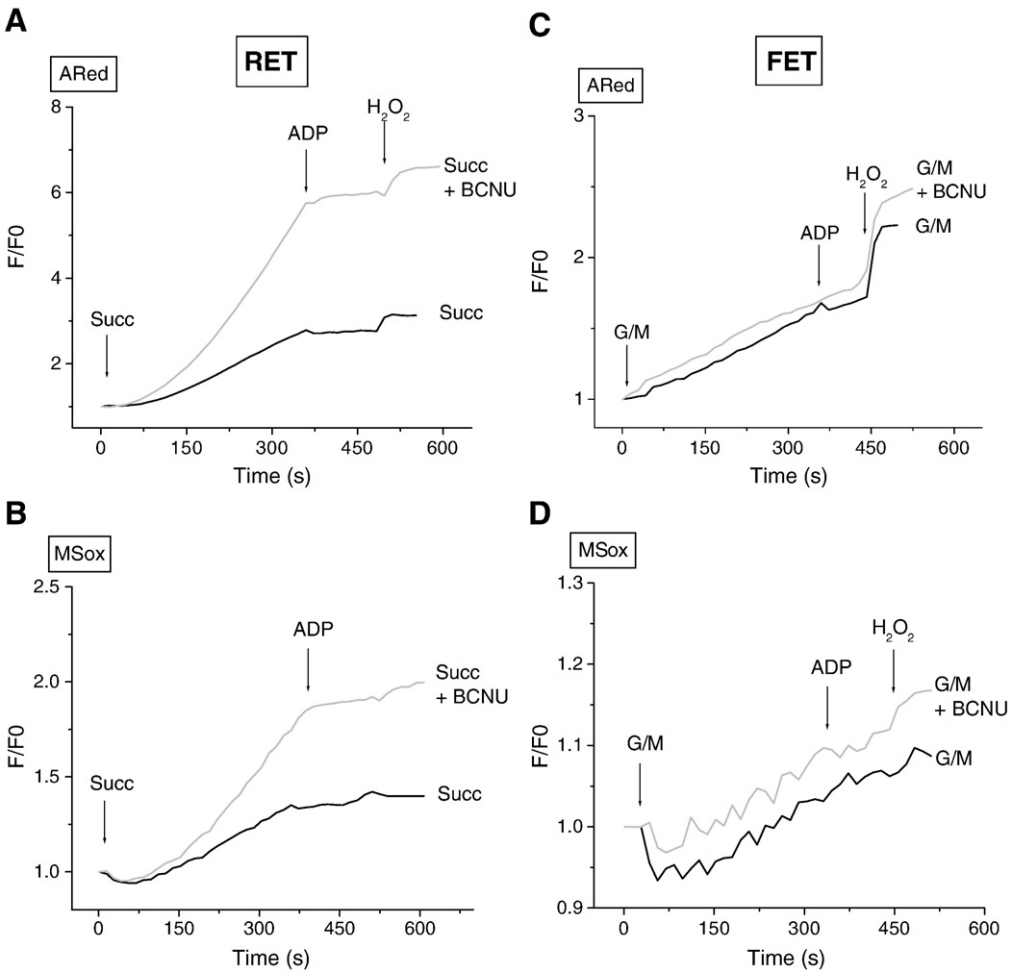

Fig. 6. Effect of inhibiting intramitochondrial GSH regeneration on the mitochondrial ROS balance under FET and RET. Freshly isolated mitochondria from guinea pig heart, preloaded with 4 μM MitoSOX, were preincubated with 100 μM BCNU (carmustine), an inhibitor of glutathione reductase, and analyzed as described in the legend of Fig. 3, in the presence of ARed, both under RET (A, B) and FET (C, D).

a continuous increase in GSH in the matrix (Fig. 5B) but without a concomitant change in NADH, which was already fully reduced (not shown).

The importance of maintaining the flux through the antioxidant redox pathways on ROS balance is shown in Fig. 6. Inhibition of the glutathione reductase (GR) reaction (GSSG → 2GSH) with carmustine (BCNU) substantially increased (by approximately 2-fold) the rates of H_2O_2 (Fig. 6A) and $O_2^{\bullet-}$ (Fig. 6B) accumulation under conditions of RET; however, it had no effect on the rate of ROS generated during FET (Fig. 6C and D, respectively), suggesting that the reserve capacity of the reduced thiol pool was sufficient to effectively scavenge the lower levels of ROS produced during FET. As expected, the decline in matrix GSH is more pronounced under RET in the presence of BCNU than in its absence (see Fig. S1 in Supplementary material). Moreover, an immediate decrease in matrix GSH follows Succ addition, which then recovers to a lower steady level during the manifest increase of $O_2^{\bullet-}$ in the matrix, and H_2O_2 outside the mitochondria (see Fig. S1 in Supplementary material).

In order to further demonstrate the dynamic nature of mitochondrial ROS balance, we performed exogenous additions of H_2O_2 to mitochondria respiring in state 4, while monitoring GSH (Fig. 7A), NADH (Fig. 7B) and H_2O_2 release. The results show that the mitochondrial redox status becomes immediately and increasingly oxidized with sequential additions of exogenous H_2O_2. Notably, the presence of the exogenous ARed reporter (containing horseradish peroxidase) provides some additional scavenging capacity to the system: the extent of mitochondrial NADH and GSH oxidation was lessened in its presence and their recovery rates improved following H_2O_2 additions. This notwithstanding, increasing concentrations of H_2O_2 (i.e. >150 nM) diminished the recovery of the mitochondrial redox pools. In the range of H_2O_2 concentrations utilized, the response of mitochondria to ADP addition was not compromised, as suggested by the normal oxidation of the NADH pool (compare Figs. 3C and 7B).

Taken together, the findings illustrate how, in addition to changes in the rate of ROS production, ROS balance is highly responsive to both matrix and extra-mitochondrial scavenging systems, dynamically sensing and adjusting in response to internal and external interventions on the antioxidant defenses.

3.5. Opposite effects of uncoupling oxidative phosphorylation on ROS balance under FET in isolated versus in vivo mitochondria

We next explored the effects of low levels of mitochondrial uncoupling on isolated mitochondria and cells. Cardiomyocytes or mitochondria isolated from guinea pig hearts were subjected to increasing (nM) concentrations of the uncoupler (protonophore) FCCP while monitoring mitochondrial $\Delta\Psi_m$, NADH, and ROS ($O_2^{\bullet-}$ and H_2O_2). FCCP had opposite effects on the mitochondrial ROS release in isolated mitochondria compared with mitochondria *in situ*.

The uncoupler increased the rates of $O_2^{\bullet-}$ (Fig. 8A) and H_2O_2 (Fig. 8B) accumulation in a concentration-dependent manner (10 to 50 nM) in cardiomyocytes loaded with MitoSOX ($O_2^{\bullet-}$) and CM-DCF (H_2O_2). A summary of the results obtained with both ROS probes imaged simultaneously in cardiomyocytes from three independent

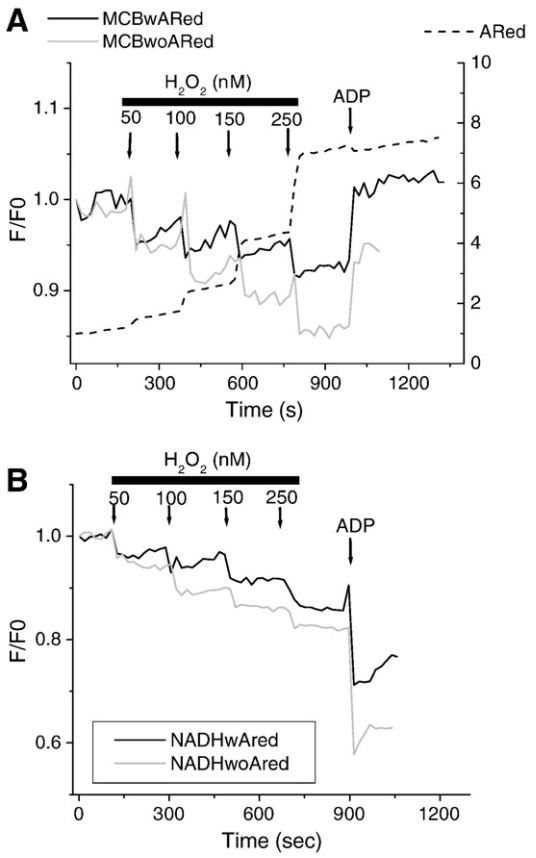

Fig. 7. Dynamic response of the mitochondrial ROS balance to pulses of H_2O_2 under FET. Freshly isolated mitochondria from guinea pig heart, preloaded with 20 μM MCB, were subjected to pulses of H_2O_2 at the indicated concentrations, under FET. GSH (A) and NAD(P)H (B) redox pools were monitored simultaneously without (grey trace) or with ARed (black trace), at state 4 respiration in the presence of 5 mM G/M or state 3 respiration after addition of 1 mM ADP. Notice the relatively lower extent of oxidation of GSH and NAD(P)H redox pools in the presence of ARed, which acts as an H_2O_2 scavenging system (see the increase photon counts exhibited in the dashed trace of panel A after each H_2O_2 pulse). Key to symbols: MCBwARed, MCB-loaded mitochondria in the presence of ARed; MCBwoARed, MCB-loaded mitochondria in the absence of ARed; NADHwARed, mitochondria in the presence of ARed; NADHwoARed, mitochondria in the absence of ARed.

experiments is shown in Fig. 8C (see also Fig. S4 from Supplementary material).

In isolated mitochondria energized with G/M (FET) in state 4, increasing concentrations of FCCP (5 to 50 nM) decreased H_2O_2 accumulation (Fig. 9). FCCP decreased the rate either with preincubation of the mitochondria (5 to 20 nM) (Fig. 9B) or during successive additions (5 to 75 nM) (Fig. 9A). The overall decrease in the rate was ~50% (Fig. 9A; see also Fig. 10). Simultaneous measurement of $\Delta\Psi_m$ and NADH shows that FCCP concomitantly uncouples $\Delta\Psi_m$ (Fig. 9C) and oxidizes NADH (Fig. 9D). A similar trend was observed in $\Delta\Psi_m$ and NADH in FCCP-preincubated mitochondria (results not shown). At concentrations 20 nM or higher, FCCP greatly decreases NADH and collapses $\Delta\Psi_m$ (Fig. 9C and D). H_2O_2 accumulation already declines noticeably in the range of 5–10 nM FCCP (Fig. 9A).

3.6. The redox-optimized ROS balance hypothesis accounts for the differences in ROS balance in isolated mitochondria and cells

Based on the results described above, in the context of the main hypothesis, it is suggested that the normal set point of operation for cells lies to the left side (more oxidized redox potential) of the minimum in the ROS balance curve and to the right side (more reduced redox potential) for isolated mitochondria (Fig. 1).

As a further validation of the hypothesis, we next examined whether the intact cell or isolated mitochondrial preparations could be pushed to the opposite arm of the ROS balance curve. In other words, could isolated mitochondria release more ROS if pushed towards the oxidized redox state and could myocytes release more ROS under highly reduced conditions?

Isolated mitochondria were, therefore, exposed to exogenous levels of H_2O_2 (μM) and the intramitochondrial GSH pool was further depleted with MCB (Fig. 10). Under these oxidizing conditions, and with FET in state 4, the effect of FCCP on ROS was reversed: graded increases in mitochondrial uncoupling increased ROS release (Fig. 10B) instead of decreasing it as in mitochondria that were not oxidatively stressed (Fig. 10A), while it produces the opposite result in non-stressed mitochondria (Figs. 9A and 10A).

Cardiomyocytes were pushed more towards the reduced state by applying the thiol reducing agent dithiothreitol (DTT) and the effects of FCCP were assessed. In the presence of DTT, mild uncoupling decreased H_2O_2 accumulation in cells (Fig. 11A) and mitochondrial matrix $O_2^{\bullet-}$ accumulation was blunted. This behavior was the opposite of that observed in cells under normal reducing conditions (Fig. 8).

Fig. 10C and D depict a summary of the results for ROS release obtained with isolated mitochondria as a function of the redox environment of either intramitochondrial NADH plus GSH (Fig. 10C) or GSH alone (Fig. 10D). As predicted in Fig. 1, a clear minimum in the curve describing the relationship between ROS released into the medium and redox potential is observed, within the normal physiological operating range of mitochondria doing physiological work, while ROS imbalance is observed at the redox extremes. It should also be noticed the asymmetry in the maximal amounts of ROS overflow determined at the right and left extremes of the curve: ~4-fold higher levels of ROS can be registered at the extreme of oxidation as compared with the extreme of reduction (Fig. 10C and D).

4. Discussion

The main contribution of the present work is to introduce a novel hypothesis to explain discrepancies concerning ROS balance for results obtained with mitochondria studied *in vitro* vs. *in situ*. The redox-optimized ROS balance hypothesis accounts for many apparently contradictory experimental observations reported previously.

The mechanisms governing ROS overflow (which we use here to describe a ROS imbalance leading to detectable levels of ROS using reporters) in the intact cell, as compared with isolated mitochondria, can be completely different. Freshly isolated cardiomyocytes have a redox potential in the middle range under normoxic conditions, and an increase in mitochondrial uncoupling, exogenous stressors, or high work conditions, can increase the detectable ROS primarily because the conserved redox cycles involved in the antioxidant defenses becomes compromised. Conversely, in energized, tightly coupled isolated mitochondria, the redox potential is high and there is ample O_2 availability (~200 μM as compared with ~3 μM in cells; see [35,36]), so there is a high probability of the respiratory carriers in the electron transport chain being reduced, with a consequent increase in ROS production. Uncoupling of oxidative phosphorylation, in this case, results in a lower probability of electron transfer to $O_2^{\bullet-}$ and a decrease in detectable ROS.

The redox couples involved in substrate oxidation (within the Krebs cycle) are closely linked to the redox couples involved in antioxidant defenses through reactions that regenerate NADPH (e.g., $NADP^+$-dependent isocitrate dehydrogenase, malic enzyme, and the NADH/NADPH transhydrogenase) (Fig. 2). Hence, it is vitally important to sustain NADH production to maintain the glutathione, thioredoxin and glutaredoxin pools in the reduced state. In isolated mitochondria under state 4 conditions, the antioxidant defenses are at a maximum, so increased ROS overflow must occur via higher production of free radicals. In intact cells under working conditions,

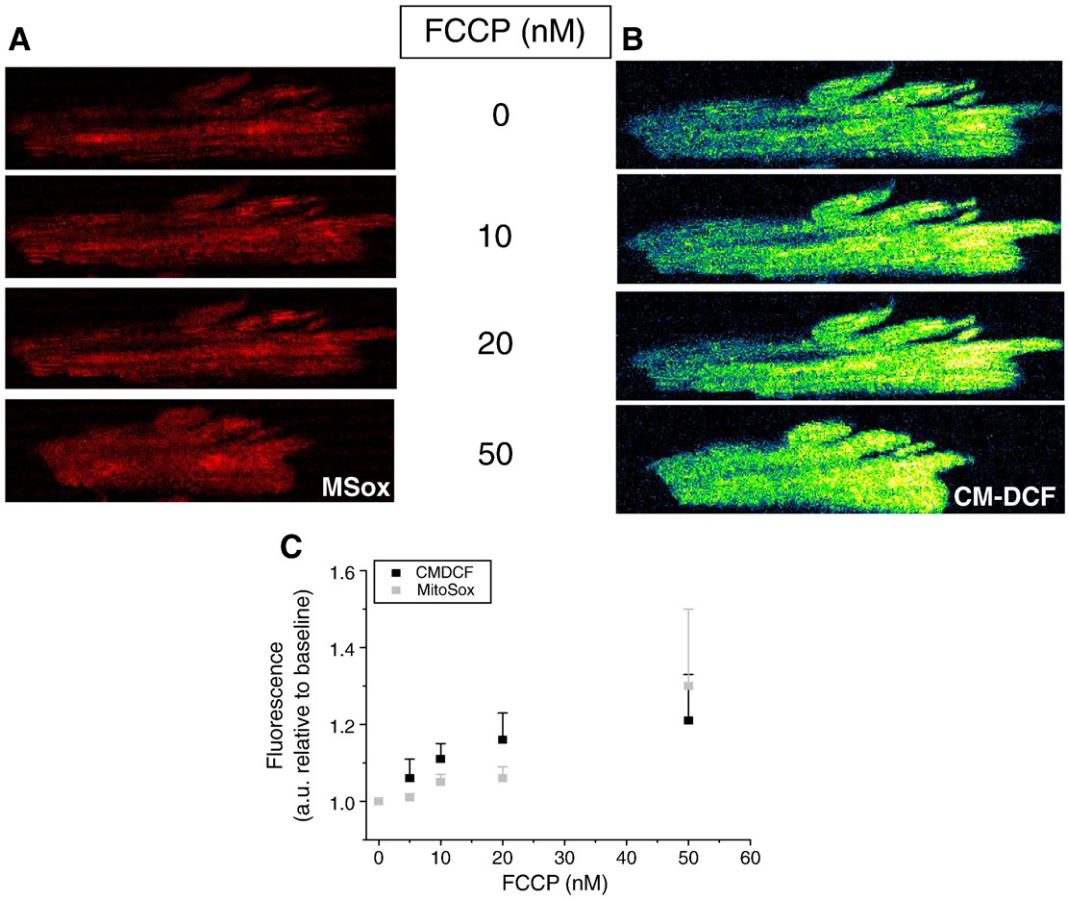

Fig. 8. Mitochondrial ROS under mild uncoupling in freshly isolated cardiomyocytes from guinea pig heart. Freshly isolated cardiomyocytes from guinea pig heart were loaded with the ROS probes MitoSOX (A) and CM-H_2DCFDA (B), and imaged with two-photon laser scanning fluorescence microscopy as described in Materials and methods. After baseline imaging of cells perfused with tyrode pH 7.5 containing 1 mM Ca^{2+} and 10 mM glucose, the indicated nanomolar concentrations of the protonophore FCCP were added. After 5 min incubation with FCCP, images were taken every 2 min, for a total of 11 min in the presence of each FCCP concentration, after which the FCCP was washed out. This experimental protocol allowed us to discern whether the effect of FCCP on mitochondrial ROS was steady, and at the same time allowed us to obtain triplicate fluorescence determinations. All observations were paired, i.e., performed in the same cells at all uncoupler concentrations, for all the experiments. Although most of the cardiomyocytes survived the FCCP treatment, some cells exhibited hypercontracture and death as expected from depletion of cytoplasmic ATP levels (see Fig. S4 from Supplementary material). Panel C shows the results obtained from three independent experiments with $n=9$ for each FCCP concentration and fluorescent probe. The fluorescence measurements corresponding to cells undergoing hypercontracture were not considered in the statistics, since the increase in fluorescence would be an artifact resulting from changes in cell shape.

the mitochondrial ROS balance is mainly determined by the antioxidant defenses. Only during hypoxia would a cell begin to approach the NAD(P)H/NAD(P)$^+$ redox potential favoring an increase in ROS overflow through the mechanisms described in state 4 isolated mitochondria.

An important validation of our hypothesis was achieved by exploring the effects of partial mitochondrial uncoupling on cells and isolated mitochondria under different redox conditions and different energy states, to reveal the relationship between mitochondrial respiration, $\Delta\Psi_m$, NADH, GSH and ROS. Mainstream thinking about this subject is based on evidence obtained with isolated mitochondria, wherein small increases in respiratory rates and $\Delta\Psi_m$ are typically accompanied by a substantial decrease in ROS release [20,37]. The "mild uncoupling" hypothesis [38], or "uncoupling to survive" [39], were postulated to be a central mechanism through which oxidant production is controlled in mitochondria, preventing oxidative damage and aging [1]. Here, we show that this situation applies only to the specific condition of very high redox potentials (Fig. 10). Mild uncoupling of the cardiomyocyte, in fact, increased ROS accumulation, in cells with physiological basal redox potentials (Fig. 8). Cells could be pushed towards the reduced redox extreme (Fig. 1) with the reducing agent DTT, and only then did ROS decrease with mild uncoupling (Fig. 11). Conversely, we showed that in oxidatively stressed mitochondria pushed to the opposite redox extreme, FCCP can increase ROS release, consequent to a decrease in antioxidant redox reserve (Fig. 10B).

4.1. Relative role of ROS overflow under FET versus RET

Since the normal physiological condition is for forward electron transport (FET), our main interest is to describe how ROS overflow can occur under FET. Nevertheless, high levels of ROS release can be also observed under RET [27,40,41]. Isolated mitochondria oxidizing the complex II substrate succinate (in the absence of rotenone) produced, in our hands, approximately 6-fold higher amounts of ROS during RET in mitochondria in state 4, as compared to those energized with complex I substrates (G/M; state 4). The rates of H_2O_2 release from the mitochondria in state 4 amounted to 1.4% and 0.6% of the oxygen consumption rate for RET and FET, respectively (Fig. 4A). For both transport modes, in agreement with earlier studies [21,27,42,43], the rate of ROS release decreased to a low (but nonzero) level upon transition to state 3, and the rates of H_2O_2 release represented ~0.02% of respiration for both RET and FET. This decrease in ROS release during the state 4→3 transition is completely dependent on ADP uptake and phosphorylation, since it was blocked by carboxyatractyloside or oligomycin (results not shown). It is important to note that in cells and tissues, and particularly the heart, the normal operating range is

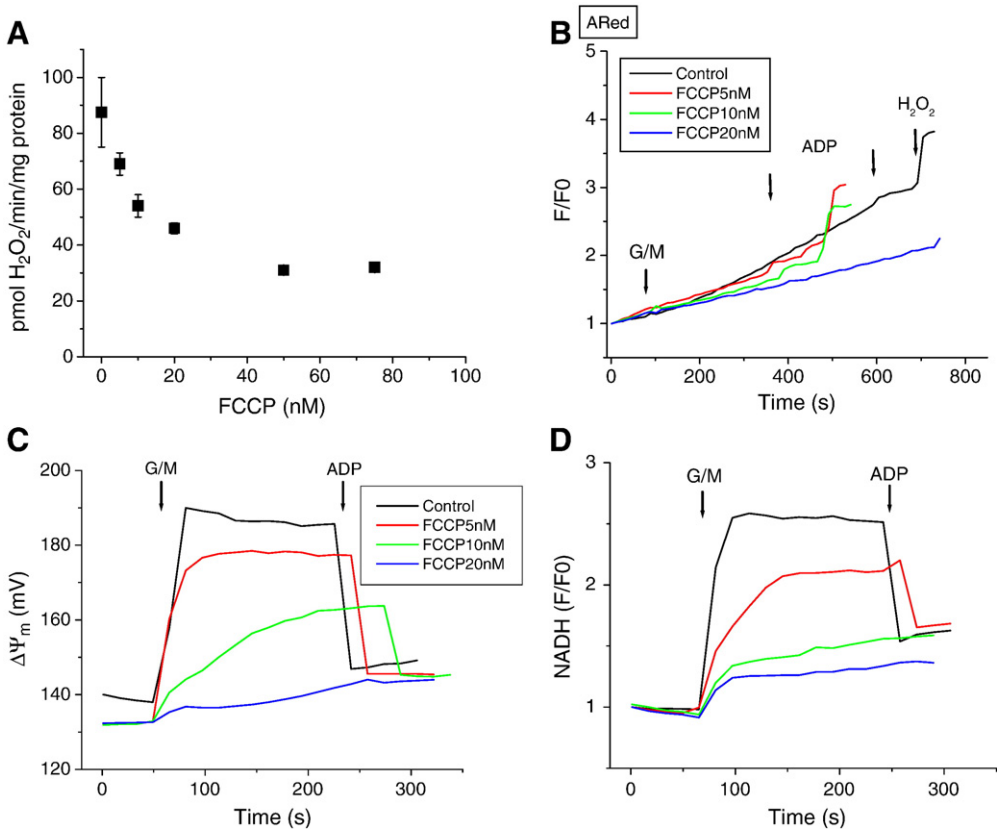

Fig. 9. ROS decreases in isolated mitochondria from guinea pig heart subjected to mild uncoupling. Freshly isolated mitochondria from guinea pig hearts were assayed as described in the legend of Fig. 3 under FET at state 4 and 3 of respiration according to additions indicated by arrows. The experiment was performed either by preincubating the mitochondria with FCCP and triggering ROS production with the substrate, or by successive addition of different concentrations of the uncoupler after energization with substrate. In panel A, the FCCP dose–response curve for mitochondrial ROS is shown for successive additions of the uncoupler ($n=4$ for each data point, 2 experiments), whereas in panel B, the raw ARed traces obtained after preincubating the mitochondria with the indicated FCCP concentrations is shown. Panels C and D show the behavior of $\Delta\Psi_m$ and NAD(P)H, respectively, for the same experiment shown in panel B.

closer to the state 3 condition: thus, the dramatic decrease in ROS overflow could be viewed as an evolutionary adaptation to minimize ROS release and maximize energy output. ROS release in RET is very much higher than for FET despite the fact that the extent of NADH reduction, VO_2 and $\Delta\Psi_m$ are similar (Fig. 3). ROS production by FET is much less sensitive to $\Delta\Psi_m$ dissipation [43–45], but is strongly increased by inhibitors of the respiratory chain, such as rotenone [21], and antimycin A ([46]; see Fig. S2 in Supplementary material, and [27] for a recent review), which decrease $\Delta\Psi_m$. In the context of the redox-optimized hypothesis, ROS overflow in the reduced state is less dependent on the idea that a high $\Delta\Psi_m$ is responsible to ROS release [37], but rather reflects the concentration and overall oxidation state of the redox couples. Additionally, increasing O_2 consumption prevents ROS formation because more oxidized levels of respiratory complexes (CI and CIII) and lower levels of NADH, are favored [47]. These data are consistent with earlier findings and the hypothesis that oxidation of the respiratory complexes by mild uncoupling can decrease ROS overflow ([48]; see also [47], and refs. therein), provided that strong antioxidant defenses are present (right side branch in Fig. 1).

With respect to earlier measurements of ROS release rates in isolated mitochondria, our findings are consistent with numerous reports, including H_2O_2 levels detected under RET and FET [21]; the increase in H_2O_2 following the addition of respiratory inhibitors both under RET and FET [37,40,49]; H_2O_2 levels detected under RET at different succinate concentrations ([50] and see Fig. S3 in Supplementary material); as well as the extent of $\Delta\Psi_m$ polarization upon G/M or Succ addition, or $\Delta\Psi_m$ depolarization when ADP was added [27,41]. Rates of $O_2^{\bullet-}$ production followed a precursor-product relationship between $O_2^{\bullet-} \rightarrow H_2O_2$ (see Fig. 3D and E) and Cadenas and Davies [51] calculated rates of 0.57×10^{-6} M s^{-1} and 0.28×10^{-6} M s^{-1} for $O_2^{\bullet-}$ and H_2O_2 production, respectively. Using our data (Fig. 4) we arrive at similar values of 0.5×10^{-6} M s^{-1} for H_2O_2 under FET, while under RET these values increased about six-fold to 3×10^{-6} M s^{-1}.

4.2. Explanatory power of the redox-optimized ROS balance in the context of physiology and pathophysiology

While some of the conditions described above for isolated mitochondria are not physiological, the right arm of the redox extreme curve is relevant to certain pathophysiological states. For example, mitochondrial ROS increases during hypoxia (decreasing ambient O_2 from 21% to 3%) [52,53], a paradoxical finding because it seems to contradict the dependence of $O_2^{\bullet-}$ production on O_2 concentration [54]. A functional respiratory chain is required [55], and, depending on the duration and extent of the hypoxia, the event can either trigger the HIF-1 transcriptional signaling response [56] or lead to cell injury, for example, neuronal cell death mediated by complex I inhibition or damage [57]. Our hypothesis would interpret these responses as the cells operating in FET on the right arm of the redox extreme curve, either in the signaling or the injury sectors. Isolated mitochondria or hypoxic cells, and perhaps even tissues subject to "reductive stress" [58], would exhibit highly reduced redox potentials and augmented $O_2^{\bullet-}$ production due to the low electron flow. The increased probability of free radical production by electron diversion at the level of the respiratory complexes could then be relieved by partial oxidation of the redox couples, for instance, by overexpressing mitochondrial uncoupling proteins [59]. This redox

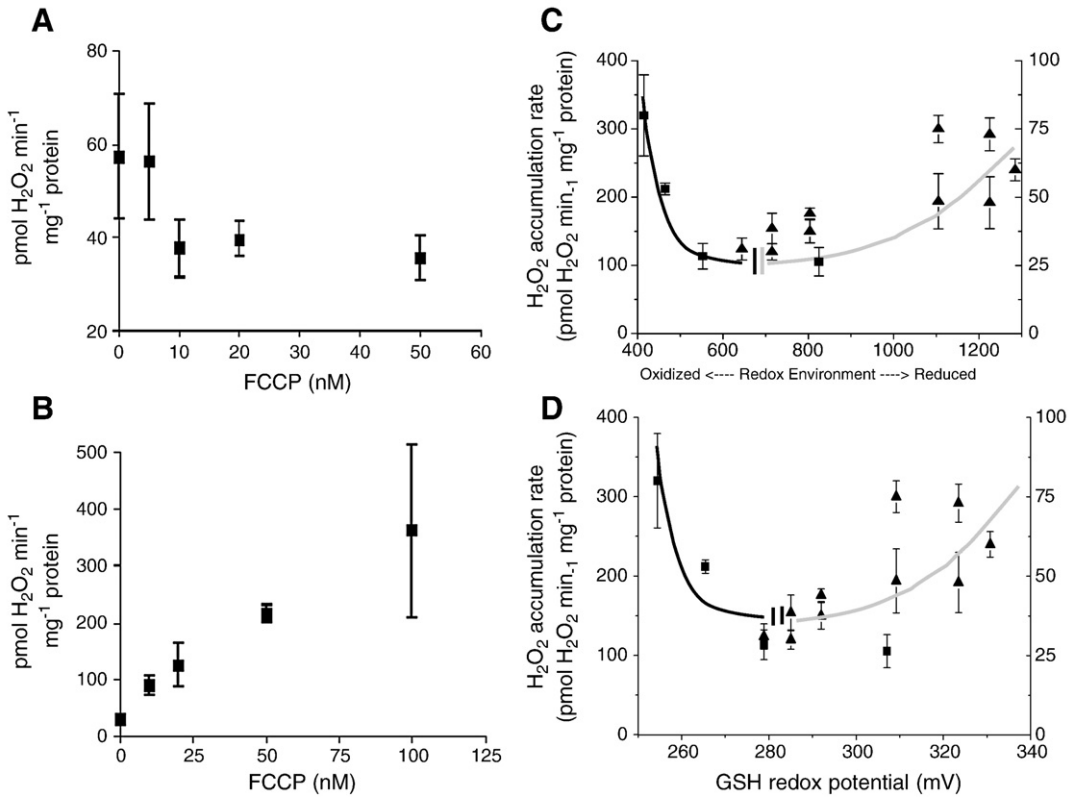

Fig. 10. Mild uncoupling can increase or decrease mitochondrial ROS depending on the redox environment in isolated mitochondria from guinea pig heart. Freshly isolated mitochondria from guinea pig heart loaded with 20 μM monochlorobimane (MCB) (A) or higher (B) were uncoupled with the indicated concentration of FCCP under FET (5 mM G/M) and state 4 respiration. A similar experiment to that reported in Fig. 9A and B is shown in panel A ($n=4$ for each data point; 2 experiments), while in panel B represented are the results obtained with mitochondria loaded with 50 μM or 100 μM MCB, preincubated with 500 nM H_2O_2, and then subjected to increasing dose of FCCP ($n=4$ for each data point; 2 experiments). Higher concentrations of MCB (>20 μM) were utilized to titrate the mitochondrial GSH pool, and further compromise the antioxidant defenses. C, D) Panels A and B plot the results as a function of the redox environment for either the NADH/NAD^+ and GSH/GSSG redox couples, calculated according to Eq. (1) (C), or the GSH/GSSG redox potential (D) obtained from Eq. (2). Squares and triangles in panels C and D correspond to the specific rates of H_2O_2 detection measured in panels A and B, respectively, as a function of the redox environment. The redox potential of the NADH/NAD^+ and GSH/GSSG redox couples in mitochondria was calculated according to Eqs. (2) and (3) from the results obtained with mitochondria loaded with MCB, recorded simultaneously with NADH as a function of increasing concentrations of FCCP. Notice the agreement of the general shape of the curves in panels C and D with the one predicted by the redox-optimized ROS balance hypothesis shown in Fig. 1.

dependence would hold true as long as O_2 itself did not become limiting for ROS production, which has been previously examined in isolated liver mitochondria subjected to low O_2 concentrations [60].

Interestingly, increased ROS release during hypoxia cannot be simply described by enhanced electron transfer to $O_2^{\bullet-}$ at complex I as a result of NADH reduction, since the $O_2^{\bullet-}$ appears to be generated at complex III (inhibited by myxothiazol) [9]. The more comprehensive view of the redox-optimized ROS balance hypothesis, which would include the QH_2/QH redox couple, could account for this observation if the occupancy of the ubisemiquinone state were elevated by a linked (currently undetermined) pathway.

In this study, we show that isolated mitochondria can also be pushed to the left (more oxidized) arm of the redox extreme curve by the application of exogenous ROS. In that case, chemical or physiological uncoupling (e.g. higher cytosolic Ca^{2+}, higher uncoupling protein expression, elevated free fatty acids) can, in fact, increase mitochondrial ROS release (Fig. 10B). In addition, state 4 and state 3 respiratory rates can be enhanced in mitochondria respiring solely on endogenous electron donors if the ROS scavengers, catalase and N-acetyl cysteine, are present [61]. This suggests that the NADH being formed by the Krebs cycle may be partially redirected to regenerating antioxidant defenses (e.g. through NADPH formation) in an effort to keep low matrix H_2O_2 levels. When substrates are provided exogenously, the surplus of redox equivalents can supply both the antioxidant defenses and the respiratory chain, again emphasizing the coupling between the redox pairs involved in oxidative phosphorylation and the antioxidant pathways (Fig. 2). The crosstalk between the conserved redox cycles linking metabolism and the antioxidant pathways is also exemplified in our studies examining the role of mitochondrial Na^+ and Ca^{2+} dynamics in maintaining the balance of energy supply and demand in cardiomyocytes from normal [62,63] or failing hearts [64]. During abrupt increases in work in the presence of high Na^+, the rate of NADH oxidation can exceed the rate of NADH production by the Krebs cycle (due to impaired Ca^{2+} accumulation by the mitochondria), resulting in a net oxidation of the NADH/NAD^+ redox couple. Coupling to the antioxidant redox pathway then results in a marked increase in oxidative stress, owing to the depletion of the antioxidant capacity. This is well accounted for by the cells being pushed towards the left arm of more oxidized redox environment. Similarly, operation on the left arm of curve could account for N-methyl D-aspartate-induced excitoxicity in neurons, whereby inhibitors of electron transport (e.g., rotenone) decrease, and mild uncoupling (FCCP) increases, ROS accumulation [65].

In intact resting cardiomyocytes under oxidative stress, we have previously shown that complex III appears to be the main source of mitochondrial $O_2^{\bullet-}$, and subsequently H_2O_2, accumulation [11]. Moreover, the phase relationship between ROS production and $\Delta\Psi_m$ revealed that an increase in the rate of ROS accumulation correlates with both $\Delta\Psi_m$ depolarization and NADH oxidation [31]. Similarly, others have shown increases in the oxidation of fluorescent ROS reporters accompanying $\Delta\Psi_m$ depolarization during ROS-induced

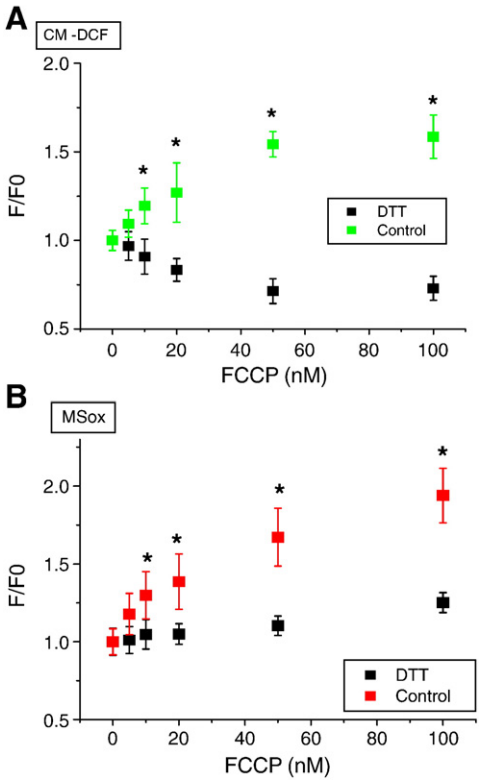

Fig. 11. Mild uncoupling can increase or decrease mitochondrial ROS depending on the redox environment in isolated cardiomyocytes from guinea pig heart. Freshly isolated cardiomyocytes from guinea pig heart were handled, and loaded with the ROS probes CM-H_2DCFDA (A) and MitoSOX (B) and imaged with two-photon scanning laser fluorescence microscopy as described in Materials and methods and the legend of Fig. 8. After baseline imaging of cells in the absence or the presence of 1 mM or 2 mM dithiothreitol (DTT) perfused with tyrode pH 7.5 containing 1 mM Ca^{2+} and 10 mM glucose, the indicated nanomolar concentrations of the protonophore FCCP were added. Identical imaging protocol to that described in Fig. 8 was followed in the FCCP dose–response. Data for control or DTT pretreated cells were paired, i.e. performed in the same cells at all uncoupler concentrations, all throughout the experiment ($n=6$ for each FCCP concentration; 2 experiments). $^*p<0.05$.

ROS release [10,11,66]. This relationship could occur either because the rate of ROS production by the electron transport chain increases with depolarization, and previous evidence indeed supports a positive correlation between ROS production and respiratory rate from complex III [46,67], or by oxidation of the antioxidant pool subsequent to NAD(P)H oxidation. Based on the former idea, we modeled ROS production accordingly, i.e., ROS production was assumed to be proportional to the rate of respiration (VO_2). This approximation was consistent with our experimental observations concerning the relationship between ROS production and $\Delta\Psi_m$ during metabolic oscillations in intact myocytes [11] and the computational model behavior described low $O_2^{\bullet-}$ production in state 4 and an increase in state 3, or when energy dissipating inner membrane channels were open. Although our model included the antioxidant defenses in the cytoplasm, our explanation now appears to be incomplete in the light of the current hypothesis, since the left arm of the ROS balance curve is not adequately represented. By being poised near the minimum of the curve in Fig. 1, compromising the antioxidant defenses of the cell could contribute significantly to the positive increase in mitochondrial ROS accumulation in lieu of, or in addition to, an increase in ROS production by the electron transport chain. Similarly, our previous work demonstrating that ROS accumulation is enhanced, and mitochondrial depolarization is triggered, when the GSH/GSSG ratio is lowered by diamide [14,18,30] is further evidence that the antioxidant redox couples are closely linked to the metabolic redox couples (NADH, $FADH_2$).

5. Concluding remarks

Overall, the present findings, and available evidence from the literature, highlight the importance of considering both ROS production and ROS scavenging as the keys to understanding intracellular redox balance. According to the redox-optimized ROS balance hypothesis, pathophysiological ROS overflow would occur at the extremes of cellular redox potential, away from the optimal, intermediate, redox environment. Physiological ROS signaling would then occur when there are less extreme deviations away from the minimum, either in the more reduced or more oxidized directions. This behavioral domain would be compatible with the utilization of ROS for signaling under a variety of conditions, for example, during increased work or decreased O_2 availability, while maintaining a high mitochondrial energetic output. Consequently, under normal physiological conditions, redox-optimized ROS balance obeys the fundamental and powerful evolutionary drive toward maximal energy output and the essential ROS-dependent signaling function of mitochondria.

Acknowledgements

This work was supported by NIH grants P01HL081427 and R37HL54598.

We thank Dr. David Lloyd (University of Wales) for critically reading an earlier version of this work.

Appendix A. Supplementary data

Supplementary data associated with this article can be found, in the online version, at doi:10.1016/j.bbabio.2010.02.016.

References

[1] R.S. Balaban, S. Nemoto, T. Finkel, Mitochondria, oxidants, and aging, Cell 120 (2005) 483–495.
[2] D. Harman, Aging: a theory based on free radical and radiation chemistry, J. Gerontol. 11 (1956) 298–300.
[3] R. Pearl, The Rate of Living, University of London Press, London, 1928.
[4] R. Kelley, T. Ideker, Genome-wide fitness and expression profiling implicate Mga2 in adaptation to hydrogen peroxide, PLoS Genet. 5 (2009) e1000488.
[5] S.J. Lin, M. Kaeberlein, A.A. Andalis, L.A. Sturtz, P.A. Defossez, V.C. Culotta, G.R. Fink, L. Guarente, Calorie restriction extends *Saccharomyces cerevisiae* lifespan by increasing respiration, Nature 418 (2002) 344–348.
[6] T.J. Schulz, K. Zarse, A. Voigt, N. Urban, M. Birringer, M. Ristow, Glucose restriction extends *Caenorhabditis elegans* life span by inducing mitochondrial respiration and increasing oxidative stress, Cell Metab. 6 (2007) 280–293.
[7] V. Adam-Vizi, Production of reactive oxygen species in brain mitochondria: contribution by electron transport chain and non-electron transport chain sources, Antioxid. Redox Signal. 7 (2005) 1140–1149.
[8] C.P. Baines, M. Goto, J.M. Downey, Oxygen radicals released during ischemic preconditioning contribute to cardioprotection in the rabbit myocardium, J. Mol. Cell. Cardiol. 29 (1997) 207–216.
[9] T.L. Vanden Hoek, L.B. Becker, Z. Shao, C. Li, P.T. Schumacker, Reactive oxygen species released from mitochondria during brief hypoxia induce preconditioning in cardiomyocytes, J. Biol. Chem. 273 (1998) 18092–18098.
[10] D.B. Zorov, C.R. Filburn, L.O. Klotz, J.L. Zweier, S.J. Sollott, Reactive oxygen species (ROS)-induced ROS release: a new phenomenon accompanying induction of the mitochondrial permeability transition in cardiac myocytes, J. Exp. Med. 192 (2000) 1001–1014.
[11] M.A. Aon, S. Cortassa, E. Marban, B. O'Rourke, Synchronized whole cell oscillations in mitochondrial metabolism triggered by a local release of reactive oxygen species in cardiac myocytes, J. Biol. Chem. 278 (2003) 44735–44744.
[12] M.A. Aon, S. Cortassa, B. O'Rourke, Percolation and criticality in a mitochondrial network, Proc. Natl. Acad. Sci. U. S. A. 101 (2004) 4447–4452.
[13] F.G. Akar, M.A. Aon, G.F. Tomaselli, B. O'Rourke, The mitochondrial origin of postischemic arrhythmias, J. Clin. Invest. 115 (2005) 3527–3535.
[14] M.A. Aon, S. Cortassa, F.G. Akar, D.A. Brown, L. Zhou, B. O'Rourke, From mitochondrial dynamics to arrhythmias, Int. J. Biochem. Cell Biol. 41 (2009) 1940–1948.
[15] M.A. Aon, S. Cortassa, B. O'Rourke, Mitochondrial oscillations in physiology and pathophysiology, Adv. Exp. Med. Biol. 641 (2008) 98–117.
[16] D.A. Brown, M.A. Aon, F.G. Akar, T. Liu, N. Sorarrain, B. O'Rourke, Effects of 4′-chlorodiazepam on cellular excitation–contraction coupling and ischaemia–reperfusion injury in rabbit heart, Cardiovasc. Res. 79 (2008) 141–149.

[17] B. O'Rourke, S. Cortassa, M.A. Aon, Mitochondrial ion channels: gatekeepers of life and death, Physiology (Bethesda) 20 (2005) 303–315.
[18] M.K. Slodzinski, M.A. Aon, B. O'Rourke, Glutathione oxidation as a trigger of mitochondrial depolarization and oscillation in intact hearts, J. Mol. Cell. Cardiol. 45 (2008) 650–660.
[19] S. Miwa, M.D. Brand, Mitochondrial matrix reactive oxygen species production is very sensitive to mild uncoupling, Biochem. Soc. Trans. 31 (2003) 1300–1301.
[20] V.P. Skulachev, Uncoupling: new approaches to an old problem of bioenergetics, Biochim. Biophys. Acta 1363 (1998) 100–124.
[21] Y. Kushnareva, A.N. Murphy, A. Andreyev, Complex I-mediated reactive oxygen species generation: modulation by cytochrome c and NAD(P)+ oxidation-reduction state, Biochem. J. 368 (2002) 545–553.
[22] Z. Radak, H.Y. Chung, S. Goto, Systemic adaptation to oxidative challenge induced by regular exercise, Free Radic. Biol. Med. 44 (2008) 153–159.
[23] F.R. Heinzel, Y. Luo, G. Dodoni, K. Boengler, F. Petrat, F. Di Lisa, H. de Groot, R. Schulz, G. Heusch, Formation of reactive oxygen species at increased contraction frequency in rat cardiomyocytes, Cardiovasc. Res. 71 (2006) 374–382.
[24] I.J. Reynolds, T.G. Hastings, Glutamate induces the production of reactive oxygen species in cultured forebrain neurons following NMDA receptor activation, J. Neurosci. 15 (1995) 3318–3327.
[25] R.A. Forbes, C. Steenbergen, E. Murphy, Diazoxide-induced cardioprotection requires signaling through a redox-sensitive mechanism, Circ. Res. 88 (2001) 802–809.
[26] J.P. Brennan, R. Southworth, R.A. Medina, S.M. Davidson, M.R. Duchen, M.J. Shattock, Mitochondrial uncoupling, with low concentration FCCP, induces ROS-dependent cardioprotection independent of KATP channel activation, Cardiovasc. Res. 72 (2006) 313–321.
[27] P. Schonfeld, L. Wojtczak, Fatty acids as modulators of the cellular production of reactive oxygen species, Free Radic. Biol. Med. 45 (2008) 231–241.
[28] M.A. Aon, S. Cortassa, A.C. Wei, M. Grunnet, B. O'Rourke, Energetic performance is improved by specific activation of K(+) fluxes through K(Ca) channels in heart mitochondria, Biochim. Biophys. Acta 1797 (2010) 71–80.
[29] R.C. Scaduto Jr., L.W. Grotyohann, Measurement of mitochondrial membrane potential using fluorescent rhodamine derivatives, Biophys. J. 76 (1999) 469–477.
[30] M.A. Aon, S. Cortassa, C. Maack, B. O'Rourke, Sequential opening of mitochondrial ion channels as a function of glutathione redox thiol status, J. Biol. Chem. 282 (2007) 21889–21900.
[31] S. Cortassa, M.A. Aon, R.L. Winslow, B. O'Rourke, A mitochondrial oscillator dependent on reactive oxygen species, Biophys. J. 87 (2004) 2060–2073.
[32] B. Chance, G.R. Williams, A method for the localization of sites for oxidative phosphorylation, Nature 176 (1955) 250–254.
[33] F.Q. Schafer, G.R. Buettner, Redox environment of the cell as viewed through the redox state of the glutathione disulfide/glutathione couple, Free Radic. Biol. Med. 30 (2001) 1191–1212.
[34] R. Liu, B. Li, S.W. Flanagan, L.W. Oberley, D. Gozal, M. Qiu, Increased mitochondrial antioxidative activity or decreased oxygen free radical propagation prevent mutant SOD1-mediated motor neuron cell death and increase amyotrophic lateral sclerosis-like transgenic mouse survival, J. Neurochem. 80 (2002) 488–500.
[35] E. Gnaiger, B. Lassnig, A.V. Kuznetsov, R. Margreiter, Mitochondrial respiration in the low oxygen environment of the cell. Effect of ADP on oxygen kinetics, Biochim. Biophys. Acta 1365 (1998) 249–254.
[36] E. Gnaiger, G. Mendez, S.C. Hand, High phosphorylation efficiency and depression of uncoupled respiration in mitochondria under hypoxia, Proc. Natl. Acad. Sci. U. S. A. 97 (2000) 11080–11085.
[37] S.S. Korshunov, V.P. Skulachev, A.A. Starkov, High protonic potential actuates a mechanism of production of reactive oxygen species in mitochondria, FEBS Lett. 416 (1997) 15–18.
[38] V.P. Skulachev, Role of uncoupled and non-coupled oxidations in maintenance of safely low levels of oxygen and its one-electron reductants, Q. Rev. Biophys. 29 (1996) 169–202.
[39] M.D. Brand, Uncoupling to survive? The role of mitochondrial inefficiency in ageing, Exp. Gerontol. 35 (2000) 811–820.
[40] A.Y. Andreyev, Y.E. Kushnareva, A.A. Starkov, Mitochondrial metabolism of reactive oxygen species, Biochemistry (Mosc) 70 (2005) 200–214.
[41] P. Schonfeld, L. Wojtczak, Fatty acids decrease mitochondrial generation of reactive oxygen species at the reverse electron transport but increase it at the forward transport, Biochim. Biophys. Acta 1767 (2007) 1032–1040.
[42] M.D. Brand, C. Affourtit, T.C. Esteves, K. Green, A.J. Lambert, S. Miwa, J.L. Pakay, N. Parker, Mitochondrial superoxide: production, biological effects, and activation of uncoupling proteins, Free Radic. Biol. Med. 37 (2004) 755–767.
[43] A.A. Starkov, G. Fiskum, Regulation of brain mitochondrial H2O2 production by membrane potential and NAD(P)H redox state, J. Neurochem. 86 (2003) 1101–1107.
[44] L. Tretter, V. Adam-Vizi, Uncoupling is without an effect on the production of reactive oxygen species by in situ synaptic mitochondria, J. Neurochem. 103 (2007) 1864–1871.
[45] T.V. Votyakova, I.J. Reynolds, DeltaPsi(m)-Dependent and -independent production of reactive oxygen species by rat brain mitochondria, J. Neurochem. 79 (2001) 266–277.
[46] J.F. Turrens, A. Alexandre, A.L. Lehninger, Ubisemiquinone is the electron donor for superoxide formation by complex III of heart mitochondria, Arch. Biochem. Biophys. 237 (1985) 408–414.
[47] A.J. Kowaltowski, N.C. de Souza-Pinto, R.F. Castilho, A.E. Vercesi, Mitochondria and reactive oxygen species, Free Radic. Biol. Med. 47 (2009) 333–343.
[48] L. Tretter, V. Adam-Vizi, Moderate dependence of ROS formation on DeltaPsim in isolated brain mitochondria supported by NADH-linked substrates, Neurochem. Res. 32 (2007) 569–575.
[49] A.J. Lambert, J.A. Buckingham, H.M. Boysen, M.D. Brand, Diphenyleneiodonium acutely inhibits reactive oxygen species production by mitochondrial complex I during reverse, but not forward electron transport, Biochim. Biophys. Acta 1777 (2008) 397–403.
[50] R.G. Hansford, B.A. Hogue, V. Mildaziene, Dependence of H2O2 formation by rat heart mitochondria on substrate availability and donor age, J. Bioenerg. Biomembr. 29 (1997) 89–95.
[51] E. Cadenas, K.J. Davies, Mitochondrial free radical generation, oxidative stress, and aging, Free Radic. Biol. Med. 29 (2000) 222–230.
[52] E.L. Bell, T.A. Klimova, J. Eisenbart, P.T. Schumacker, N.S. Chandel, Mitochondrial reactive oxygen species trigger hypoxia-inducible factor-dependent extension of the replicative life span during hypoxia, Mol. Cell. Biol. 27 (2007) 5737–5745.
[53] N.S. Chandel, E. Maltepe, E. Goldwasser, C.E. Mathieu, M.C. Simon, P.T. Schumacker, Mitochondrial reactive oxygen species trigger hypoxia-induced transcription, Proc. Natl. Acad. Sci. U. S. A. 95 (1998) 11715–11720.
[54] M.P. Murphy, How mitochondria produce reactive oxygen species, Biochem. J. 417 (2009) 1–13.
[55] R.D. Guzy, B. Hoyos, E. Robin, H. Chen, L. Liu, K.D. Mansfield, M.C. Simon, U. Hammerling, P.T. Schumacker, Mitochondrial complex III is required for hypoxia-induced ROS production and cellular oxygen sensing, Cell Metab. 1 (2005) 401–408.
[56] N.S. Chandel, D.S. McClintock, C.E. Feliciano, T.M. Wood, J.A. Melendez, A.M. Rodriguez, P.T. Schumacker, Reactive oxygen species generated at mitochondrial complex III stabilize hypoxia-inducible factor-1alpha during hypoxia: a mechanism of O2 sensing, J. Biol. Chem. 275 (2000) 25130–25138.
[57] L. Tretter, I. Sipos, V. Adam-Vizi, Initiation of neuronal damage by complex I deficiency and oxidative stress in Parkinson's disease, Neurochem. Res. 29 (2004) 569–577.
[58] N.S. Rajasekaran, P. Connell, E.S. Christians, L.J. Yan, R.P. Taylor, A. Orosz, X.Q. Zhang, T.J. Stevenson, R.M. Peshock, J.A. Leopold, W.H. Barry, J. Loscalzo, S.J. Odelberg, I.J. Benjamin, Human alpha B-crystallin mutation causes oxido-reductive stress and protein aggregation cardiomyopathy in mice, Cell 130 (2007) 427–439.
[59] C.J. McLeod, A. Aziz, R.F. Hoyt Jr., J.P. McCoy Jr., M.N. Sack, Uncoupling proteins 2 and 3 function in concert to augment tolerance to cardiac ischemia, J. Biol. Chem. 280 (2005) 33470–33476.
[60] D.L. Hoffman, P.S. Brookes, Oxygen sensitivity of mitochondrial reactive oxygen species generation depends on metabolic conditions, J. Biol. Chem. 284 (2009) 16236–16245.
[61] P. Korge, J.N. Weiss, Redox regulation of endogenous substrate oxidation by cardiac mitochondria, Am. J. Physiol. Heart Circ. Physiol. 291 (2006) H1436–H1445.
[62] C. Maack, S. Cortassa, M.A. Aon, A.N. Ganesan, T. Liu, B. O'Rourke, Elevated cytosolic Na+ decreases mitochondrial Ca2+ uptake during excitation–contraction coupling and impairs energetic adaptation in cardiac myocytes, Circ. Res. 99 (2006) 172–182.
[63] B. O'Rourke, C. Maack, The role of Na dysregulation in cardiac disease and how it impacts electrophysiology, Drug Discov. Today Dis. Models 4 (2007) 207–217.
[64] T. Liu, B. O'Rourke, Enhancing mitochondrial Ca2+ uptake in myocytes from failing hearts restores energy supply and demand matching, Circ. Res. 103 (2008) 279–288.
[65] L.L. Dugan, S.L. Sensi, L.M. Canzoniero, S.D. Handran, S.M. Rothman, T.S. Lin, M.P. Goldberg, D.W. Choi, Mitochondrial production of reactive oxygen species in cortical neurons following exposure to N-methyl-D-aspartate, J. Neurosci. 15 (1995) 6377–6388.
[66] N.R. Brady, S.P. Elmore, J.J. van Beek, K. Krab, P.J. Courtoy, L. Hue, H.V. Westerhoff, Coordinated behavior of mitochondria in both space and time: a reactive oxygen species-activated wave of mitochondrial depolarization, Biophys. J. 87 (2004) 2022–2034.
[67] J.F. Turrens, Mitochondrial formation of reactive oxygen species, J. Physiol. 552 (2003) 335–344.